Poloidal variation of high-Z impurity density due to hydrogen minority ion cyclotron resonance heating on Alcator C-Mod

Citation: Reinke, M L, I H Hutchinson, J E Rice, N T Howard, A Bader, S Wukitch, Y Lin, et al. "Poloidal variation of high-Z impurity density due to hydrogen minority ion cyclotron resonance heating on Alcator C-Mod." Plasma Physics and Controlled Fusion 54, no. 4 (April 1, 2012): 045004.

As Published: http://dx.doi.org/10.1088/0741-3335/54/4/045004

Publisher: IOP Publishing

Persistent URL: http://hdl.handle.net/1721.1/84058

Version: Author's final manuscript: final author's manuscript post peer review, without publisher's formatting or copy editing

Poloidal variation of high-Z impurity density due to hydrogen minority ICRH on Alcator C-Mod

M.L. Reinke, I. H. Hutchinson, J.E. Rice, N. T. Howard, A. Bader, S. Wukitch, Y. Lin, D. Pace, A. Hubbard, J. W. Hughes and Y. Podpaly.

Abstract

In the Alcator C-Mod tokamak, strong, steady-state variations of molybdenum density within a flux surface are routinely observed in plasmas using hydrogen minority ion cyclotron resonant heating. In/out asymmetries, up to a factor of 2, occur with both inboard and outboard accumulation depending on the major radius of the minority resonance layer. These poloidal variations can be attributed to the impurity's high charge and large mass in neoclassical parallel force balance. The large mass enhances the centrifugal force, causing outboard accumulation while the high charge enhances ion-impurity friction and makes impurities sensitive to small poloidal variations in the plasma potential. Quantitative comparisons between existing parallel high-Z impurity transport theories and experimental results for $r/a < 0.7$ show good agreement when the resonance layer is on the high-field side of the tokamak but disagree substantially for low-field side heating. Ion-impurity friction is insufficient to explain experimental results, and the accumulation of impurity density on the inboard side of flux surface is shown to be driven by a poloidal potential variation due to magnetic trapping of non-thermal, cyclotron heated minority ions. Parallel impurity transport theory is extended to account for cyclotron effects and shown to agree with experimentally measured impurity density asymmetries.

I. INTRODUCTION

The presence of impurities in fusion plasmas is known to be a challenge because of power loss in the core from radiation and fuel dilution. Still, tokamaks use impurities to maintain radiative divertors and mantles to protect plasma facing components [1] and impurity ions that are not fully-stripped of electrons can be used to diagnose kinetic properties of plasmas. Whether used as tracers or viewed as contaminants to be eliminated, their presence is ubiquitous and the physics of high-Z impurity transport in tokamaks is still not completely understood [2]. Much effort has been focused on characterizing cross-field impurity transport [3], and as the community moves towards validation [4] of gyrokinetic modeling of the turbulence thought to be responsible [5,6], it is important to include all relevant physics. When calculating force balance along the field, the large mass and high charge of impurity ions are expected to cause variations of the impurity density on a flux surface [7,8,9]. Both neoclassical [10,11] and anomalous cross-field transport [12,13] have proven to be sensitive to the magnitude and direction of these asymmetries. Substantial poloidal variation can also lead to systematic errors when interpreting data from diagnostics sensitive to impurity emission. It is thus of interest to have a validated model for parallel impurity transport as part of the larger understanding of impurity transport in tokamaks.

Prior investigations on JET [14] and AUG [15] into high-Z impurity density asymmetries have focused on neutral beam-heated plasmas where centrifugal effects due to externally applied torque can lead to toroidal flows exceeding the impurity thermal velocity, $v_{\phi,z}/v_{th,z} \geq 1$. In these cases, the large mass of the impurities enhances the centrifugal force, causing accumulation on the outboard or low-field side (LFS) of a flux surface. In Alcator C-Mod [16] deuterium plasmas using hydrogen minority ion cyclotron resonant heating (ICRH), toroidal rotation rates up to ~20 kHz have been observed, despite no external momentum input, and such a LFS accumulation is expected for intrinsic molybdenum. Measuring the two-dimensional impurity density profile reveals that indeed such in/out asymmetries exist in C-Mod plasmas with the poloidal variation, $\tilde{\tilde{n}}_z/\langle n_z \rangle$, up to 0.3, yet measurements are not always in quantitative agreement with predictions based solely on centrifugal force. In some cases the sense of the asymmetry is even reversed, with accumulation on the inboard or high-field side (HFS) of a flux surface, indicating another physical mechanism is at work.

Impurity asymmetries have not been thoroughly investigated in wave-heated plasmas. The use of cyclotron heating is predicted to play a role in the parallel impurity force balance due to a poloidally varying electrostatic potential sustained by magnetically trapped electrons (ECRH) or ions (ICRH) [17, 18]. The high charge of the impurities magnifies any small potential variation caused by this trapping, and they respond in Boltzmann-like manner with $\tilde{\tilde{n}}_z/\langle n_z \rangle \sim \exp(-Ze\tilde{\phi}/T_z)$. In JET, Ni laser blow off into a

plasma using hydrogen minority ICRH showed a ~10 % HFS accumulation that was shown to be qualitatively consistent with estimates of magnetic trapping of minority ions [19]. Using toroidal field scans to modify the location of the minority resonance layer, C-Mod experiments discussed here demonstrate conclusively an impurity asymmetry linked to ICRH, and show measurements can be explained quantitatively by highly charged molybdenum ions interacting with a steady-state poloidal potential variation due to minority ions trapped on the LFS of the plasma.

In Section II, the physics of parallel impurity transport is briefly reviewed and current theory is extended to include effects due to cyclotron heating. Section III describes the experiments performed on the Alcator C-Mod tokamak and the diagnostic tools used to measure and model the asymmetries, with Section IV discussing the data analysis techniques. Section V presents the experimental results, qualitatively and quantitatively demonstrating the link between the changes in the asymmetries and the ICRH heating. Section VI discusses the impact of these observations while Section VII summarizes the findings.

II. THEORETICAL BACKGROUND

Existing parallel impurity transport theories solve the coupled continuity and parallel force balance equation for a collisional (Pfirsch-Schlüter) high-Z impurity for collisionless (banana) main ions [7]. In addition to inertial forces, ion-impurity friction has also been identified as a mechanism to sustain an impurity pressure gradient along the fields. While thought to be a major influence for low-Z impurities in the pedestal of C-Mod [20], ion-impurity friction cannot explain the observations of molybdenum asymmetries. The poloidal variation of n_z can be found by solving the 1-D inhomogenous differential equation, (25) in [7], in the trace, $n_z Z^2/n_i << 1$, limit

$$\frac{\partial n}{\partial \theta} = n\, g\left(1+\gamma\, b^2\right) + g\,\gamma \frac{K_z}{\langle n_z \rangle u} b^2 + n\frac{\partial M^2}{\partial \theta} \quad (1)$$

where $b^2=B^2/\langle B^2\rangle$, $n= n_z/\langle n_z\rangle$, K_z is found from the integral constraint that $n(0)=n(2\pi)$ and $\langle ... \rangle$ denotes the flux-surface average. The coefficients u, g and γ are gradient driven terms related to ion-impurity friction and main-ion poloidal flow and can be found in [7]. The M^2 term is combination of the centrifugal force on the impurities and the force from the electrostatic potential variation arising from the weaker poloidal asymmetry of the main ion density, also due to the centrifugal force.

$$M^2 = \frac{m_z \omega_z^2 R^2}{2\mathrm{T}_i}\left(1 - \frac{Z m_i}{m_z}\frac{T_e}{T_e+T_i}\right) \quad (2)$$

The effect of wave heating on the poloidal potential variation has previously not been included in

these theories. To evaluate the impact on the impurity asymmetry, a minority species is included in calculating the electrostatic potential variation on a flux surface. As discussed in [19], a cyclotron heated species can be modeled with a bi-Maxwellian distribution characterized by a temperature anisotropy, $T_\perp/T_\| > 1$. The parallel force balance equation for a species with an anisotropic but diagonal pressure tensor and a poloidally varying electrostatic potential is,

$$\hat{b}\cdot\left(\nabla\cdot\bar{P}+n_m Z_m\nabla\tilde{\phi}\right)=\nabla_\| p_\|+\frac{p_\|-p_\perp}{B}\nabla_\| B+n_m Z_m\nabla_\|\tilde{\phi}=0 \quad (3)$$

Taking the temperatures to have zero parallel gradient, (3) can be used to find the poloidal variation of the minority density, $n_m/\langle n_m\rangle$,

$$\nabla_\|\left(\ln(n_m)+\ln(B^\eta)-\frac{Z_m\tilde{\phi}}{T_\|}\right)=0$$

$$\frac{n_m}{\langle n_m\rangle}=\left\langle\frac{1}{B^\eta}\right\rangle^{-1}\frac{1}{B^\eta}\exp\left(\frac{-Z_m\tilde{\phi}}{T_\|}\right) \quad (4)$$

where $\eta=T_\perp/T_\|-1$ and B is the magnitude of the magnetic field. Including the minorities in quasi-neutrality can be done without modifying the structure of differential equation (1). Assuming a small hydrogen minority fraction, $f_m=n_m/n_e \ll 1$, $Z_m=1$ and that $e\tilde{\phi}/T_e$ is small, (2) can be replaced by,

$$M^2=\frac{m_z\omega_z^2R^2}{2T_i}\left(1-\frac{Zm_i}{m_z}\frac{T_e}{T_e+T_i}\right)-Zf_m\frac{T_e}{T_e+T_i}\left\langle\frac{1}{B^\eta}\right\rangle^{-1}\frac{1}{B^\eta} \quad (5)$$

This model assumes that the effect of the waves is to establish an anisotropic minority distribution that slows down on electrons and ions without directly impacting the parallel force balance of ions or impurities. Collisional processes will equilibrate temperatures along the field and between ion species. Using this *ansatz* requires that Z_m and f_m remain small enough that minority-impurity friction is not important.

If only inertial and electrostatic forces are important in the parallel force balance, then the poloidal variation of any thermalized ion species, main ion or impurity, will have the form,

$$n_a=\langle n_a\rangle\exp\left[\frac{-Z_a e\tilde{\Phi}}{T_a}+\frac{m_a\omega^2}{2T_a}\left(R^2-\langle R^2\rangle\right)\right] \quad (6)$$

while the electrons will exhibit a Boltzmann distribution, $n_e=\langle n_e\rangle\exp(e\tilde{\phi}/T_e)$. Inserting these density relations into quasineutrality and including the minority density described by (4), the electrostatic potential variation can be found,

$$\frac{e\tilde{\Phi}}{T_e}=\left(1+Z_{eff}\frac{T_e}{T_i}\right)^{-1}\left[f_m\left(\left\langle\frac{1}{B^\eta}\right\rangle^{-1}\frac{1}{B^\eta}-1\right)+\sum\nolimits_{j\neq m}Z_j f_j\frac{m_j\omega^2}{2T_i}\left(R^2-\langle R^2\rangle\right)\right] \quad (7)$$

where, $T_i=T_j$ and $Z_m=1$ have been assumed. For deuterium plasmas, a useful approximation can be made to account for the summation over ion species in the second part of (7), with $m_j/m_i \sim Z_j$ for fully stripped impurities, allowing Z_{eff} to be used. By inserting (7) into (6), a general equation for the poloidal variation of an ion species in a rotating, ion cyclotron-heated plasma is found.

$$\frac{n_a}{\langle n_a \rangle} = 1 + \frac{m_a \omega^2}{2T_i}\left(1 - \frac{Z_a m_i}{m_a}\frac{Z_{eff}T_e}{T_i + Z_{eff}T_e}\right)\left(R^2 - \langle R^2 \rangle\right) - Z_a f_m \frac{T_e}{T_i + Z_{eff}T_e}\left(\left\langle \frac{1}{B^\eta}\right\rangle^{-1}\frac{1}{B^\eta} - 1\right) \quad (8)$$

For the $Z_{eff}=1$ limit, numerical solutions of (1) using (5) for M^2 are shown to agree with this analytical result. In the large aspect ratio, circular limit (8) can be shown to reduce to an in/out asymmetry,

$$\frac{\tilde{n}_z}{\langle n_z \rangle} = 2\frac{r}{R_o}\cos\theta\left[\frac{m_z \omega_z^2 R_o^2}{2T_i}\left(1 - \frac{Zm_i}{m_z}\frac{Z_{eff}T_e}{T_i + Z_{eff}T_e}\right) - \frac{Zf_m}{2}\frac{T_e}{T_i + Z_{eff}T_e}\left(\frac{T_\perp}{T_\parallel} - 1\right)\right] \quad (9)$$

where the tilde indicates the poloidally varying component, $n_z = \langle n_z \rangle + \tilde{n}_z$. For molybdenum in a C-Mod deuterium plasma, $\langle Z \rangle \sim 32$. When $f_m \sim 5\%$, $T_e \approx T_i$, a temperature anisotropy of $T_\perp/T_\parallel \sim 2.7$ in the minority temperature will have as much an impact on the asymmetry as a toroidal flow of order the thermal velocity, $v_{\phi,z}/v_{z,th}$. This effect acts opposite to the centrifugal force, pushing the impurities to the HFS, and in the low-flow or high P/n_e limit ($\eta >> 1$), the effect of minority temperature anisotropy can be expected to dominate the asymmetry physics. Comparisons between theory and experiment in Section V will be done using (1) and (8) which do not make any assumptions regarding the flux-surface geometry.

III. DESCRIPTION OF EXPERIMENTS

In Alcator C-Mod plasmas where hydrogen minority heating is used, intrinsic molybdenum from plasma facing components is commonly observed at fractions of 10^{-4} to 10^{-3} and makes up the majority of the radiated power loss. In order to gain insight into the parallel impurity transport physics driven by ICRH, the flux-surface variation of this radiation is observed as the hydrogen minority, D(H), resonance layer is scanned. The heating is provided by x2 two-strap antennas at 80 and 80.5 MHz and a single four-strap antenna at 78 MHz using $(0,\pi,\pi,0)$ phasing [21]. A toroidal field of B_t=5.4 T places all frequencies approximately on-axis, R_o~0.68 m, and over consecutive discharges, the toroidal field is scanned from 4.2 T to 6.2 T, moving the resonance layer from the HFS to the LFS, as shown in Figure 1. The ICRH power, ~3 MW, and antenna mix is kept constant and the line-averaged electron density is held fixed at ~ $1.8\text{x}10^{20}$ m^{-3} using cryopumping. The plasma current is 1.1 MA in discharges with $B_t > 4.4$ T and reduced to 1.0 MA in those with smaller toroidal field in an effort to maintain a $q_{95} > 3$. All plasmas exhibit sawtooth activity and are therefore presumed to have $q_o < 1$. As the D(H) resonance location is scanned,

the electron and ion temperature profiles do not stay constant, nor does the toroidal rotation profile but all are measured. Upper single null plasmas in the unfavorable ∇B drift direction are used, which allow for high P_{ICRF}/n_e by avoiding H-mode, due to the increased L/H threshold power common in this configuration. Plasma shape is held constant over the B_t scan, and for on-axis heating, I-mode [22] plasmas are obtained while for sufficiently off-axis heating, plasmas remain in L-mode.

Profiles of the electron density and temperature are measured using Thomson scattering with additional T_e measurements from electron cyclotron emission [23]. Spatially resolved, high resolution spectra from Ar^{16+} line emission are measured using a spherically bent crystal spectrometer where tomographic techniques are used to find the local temperature and toroidal rotation [24]. The viewing geometry of the diagnostic weights equally the inboard and outboard sides of the plasma, and any in/out asymmetries in the Ar^{16+} density can be shown to have little impact on the measurements. Main-ion and impurity temperatures are assumed to be equal because $\tau_{zi}/\tau_E << 1$ for the plasma volume under investigation. The main-ion density is calculated from the electron density profile assuming a flat dilution profile based on Z_{eff} calculated from neoclassical conductivity [25]. The hydrogen to deuterium fraction, typically measured using the isotope shift in Balmer alpha, is unavailable for these USN plasmas and n_m/n_e~4% is assumed. Example kinetic profiles for $r/a < 0.9$ for both LFS and HFS off-axis heated discharges are shown in Figure 2 and are used in Section V to compare predictions from theory to experimental measurements. The difference in toroidal rotation between LFS- and HFS-heated plasmas is currently not understood, but the x-ray spectroscopy-based measurement in Figure 2d is confirmed by looking at the sawtooth precursor frequency. This oscillation is measured by B-dot coils and soft x-ray tomography, and if this n=1 mode is assumed to be stationary in the plasma rest frame, an estimate of the rotation speed at the q=1 surface can be made. The midplane emissivity profile is determined by Abel inverting the line-integrated brightness profiles measured using two separate pinhole camera, each using a single 22-channel, unfiltered AXUV diode array [26]. One camera views from $0.44 < R < 0.89$ [m] and the other from $0.65 < R < 0.92$ [m] and tangency radii for each are indicated in Figure 1. Each camera is independently aligned and calibrated, and consistent brightness profiles are observed in regions where the views overlap.

IV. ANALYSIS TECHNIQUES

The midplane emissivity profile, $\varepsilon(R)$, can be determined from the AXUV diode arrays independent of any equilibrium reconstruction. EFIT [27] is used to find the poloidally varying part of the impurity density,

$$\frac{\tilde{n}}{\langle n_z \rangle} = \frac{\varepsilon_{LFS} - \varepsilon_{HFS}}{\varepsilon_{LFS} + \varepsilon_{HFS}} \quad (10)$$

where the ε_{LFS} and ε_{HFS} are the emissivities on the same flux surface for $R > R_o$ and $R < R_o$, respectively. The use of (10) assumes that all of the emissivity is due to molybdenum radiation. Soft x-ray and VUV spectroscopy [28] are used to identify the impurities present in the plasma and radiation modeling using cooling curves [29,30] indicates that approximately 80-90% of the emissivity is due to molybdenum for $r/a < 0.8$. The physics under investigation is expected to produce smaller or negligible asymmetries for lighter, low-Z impurities and so (10) will slightly underestimate the poloidal variation of the molybdenum density. In addition (10) assumes the moments of the electron distribution, n_e and T_e, as constant on a flux surface, which is accurate for the low main-ion Mach number plasmas, $M_i^2 < 0.1$ explored here, and expecting parallel heat conduction will force poloidal symmetry of T_e. No in/out asymmetry, $\tilde{n}_z/\langle n_z \rangle \sim 0$, is measured within error bars during Mo laser blow-off injection into Ohmic plasmas where $v_{\phi,z}/v_{z,th} << 1$ in agreement with theoretical predictions. In ICRH-heated plasmas, asymmetry measurements are taken during steady-state portions of the discharge more than 200 ms after the ICRH is turned on. The pressure anisotropy of the minority ions is calculated via the TRANSP suite [31] of codes which outputs the parallel and perpendicular stored energy, from which $p_\perp/p_\parallel = E_\perp/2E_\parallel$ and is assumed to equal $T_\perp/T_\parallel$.

The impurity density variation predicted by existing theory [7] is found by solving the 1D inhomogenous linear differential equation (1) using an integrating factor approach. Poloidal gradients are determined using flux surface geometry from EFIT and integrals are performed numerically. Outputs from this code have been verified against analytical predictions in various limiting cases. Solutions using (2) for M^2 are computed and referred to as the "INERTIA" result. To compare measurements to the extended theory derived in Section II, (8) is used and labeled as the "INERTIA+ICRH" result.

V. RESULTS

The midplane emissivity profiles for a B_t=6.0 T (LFS-heated) plasma are plotted in Figure 3 against major radius (left) and versus normalized minor radius, r/a (right). Measured error bars are due to the propigation of voltage and calibration uncertainty through the Abel inversion process. Good agreement between the two independently measured emissivity profiles (AXA and AXJ) is demonstrated in the region of overlap. In the core plasma, the emissivity for $R > R_o$ is less than for $R < R_o$ on the same flux surface but this trend reversed for $r/a > 0.6$. Figure 4 uses (10) to calculate the in/out asymmetry from the AXUV diode measurements, and the radial profiles of $\tilde{n}_z/\langle n_z \rangle$ are plotted for the discharges shown in Figures 1 and 2. Differences in the measured asymmetry profiles are observed during the

toroidal field scan, most notably when the D(H) resonance is on-axis or on the LFS and $\tilde{n}_z/\langle n_z \rangle < 0$.

Predictions from parallel transport theory which includes only inertial and ion-impurity friction forces are compared to the measurements, taking into account changes in the background plasma as shown in Figure 2 and measured Z_{eff}=2.0. Error bars in the modeled asymmetries are found by propagating uncertainties in the measured kinetic profiles using the fractional error from the m=1 expansion of (1) derived in [7]. Inboard accumulation, $\tilde{n}_z/\langle n_z \rangle < 0$, is allowed in cases of strong ion-impurity friction, but modeling using experimental profiles shows that for all regions, $\tilde{n}_z/\langle n_z \rangle$ should remain positive inside of r/a ~ 0.8. The measured and modeled profiles in the B_t=4.4 T, HFS heated plasma are shown in Figure 5a and qualitative agreement is found for r/a < 0.7, although the measured asymmetry is slightly smaller. This demonstrates the ability to sustain a large, $\tilde{n}_z/\langle n_z \rangle \sim 0.3$, high-Z impurity density asymmetry caused by centrifugal force without any externally applied momentum. This same comparison is made in Figure 5b for the B_t=6.0 T, LFS heated plasma. While the experimental results agree to modeling within the uncertainty at r/a ~ 0.8, a large discrepancy is observed for 0.3 < r/a < 0.65, where the ICRH power is expected to be deposited on the LFS.

The mechanism thought to contribute the HFS accumulation is due to a poloidal electric field created by magnetically trapped minority ions whose non-thermal distribution function is sustained by absorption of cyclotron waves. For large power per particle, P_{ICRH}/n_e, resonance localization [18] should increase the perpendicular energy of the minority ions, further trapping them until their banana tips are at the D(H) resonance layer. As this layer is scanned from LFS to HFS by changing the toroidal field, resonance localization will move the orbits from deeply trapped (LFS-heating) to trapped orbits that are nearly passing (HFS-heating). It would be expected, qualitatively, that HFS heating would have less impact on parallel impurity transport. In Figure 6, measured asymmetries at r/a~0.15, 0.45 and 0.75 are plotted for the full toroidal field scan. Far off-axis, r/a~0.75, the asymmetry is relatively independent of the resonance layer, and small variation is likely due to shot-to-shot changes in ω_z, T_e and T_i. Near the magnetic axis, r/a~0.15, the sign of $\tilde{n}_z/\langle n_z \rangle$ is driven negative as the resonance layer is moved through the region; while further off-axis, in both LFS and HFS-heated cases, the core moves towards symmetry, $\tilde{n}_z/\langle n_z \rangle$=0. For mid radius, r/a~0.45, the asymmetry response differs. As the resonance layer is scanned to the LFS, $\tilde{n}_z/\langle n_z \rangle$ decreases, eventually becoming negative, similar to on-axis heating. As the layer is scanned towards the HFS, $\tilde{n}_z/\langle n_z \rangle$ becomes more positive, even as the resonance layer passes through r/a~0.45. These trends are qualitatively consistent with the resonance localization discussion.

The differences between the measured and modeled asymmetries can also be shown to be linked to ICRH dynamically as shown in Figure 7 for the LFS-heated plasma. When the input power is ramped

down during 1.40-1.42 seconds, prior to the current and field ramp down at 1.5 seconds, the measured asymmetry profiles change quickly, moving much closer to the inertial modeling shown in Figure 5b. Cross-field transport, τ_E~30 ms, is marginally slower than the fast-ion slowing down time, 20 ms, while the parallel impurity equilibration time is faster than both, ~1 ms. We postulate that when the ICRH is removed, pitch angle scattering reduces $T_\perp/T_\parallel$, and the parallel impurity equilibrium is modified before the background plasma changes significantly, relaxing the asymmetry profiles back to their steady-state values. Figure 7 shows the time history of $\tilde{\tilde{n}}_z/\langle n_z \rangle$ at r/a ~ 0.5 and 0.7 in the LFS-heated plasmas relative to core ion and electron temperatures and the toroidal rotation frequency. The largest change is near the D(H) resonance where an initial $\tilde{\tilde{n}}_z/\langle n_z \rangle$ ~ -0.15 changes to slightly positive, in agreement with inertial modeling shown earlier. Soon after, the toroidal rotation begins to drop, and over $1.44 < t < 1.50$ seconds, in/out symmetry is recovered as the inertial force weakens.

In order to provide more quantitative theoretical comparison, the pressure anisotropy from TRANSP simulations is used to model the poloidal potential variation. Figure 8 compares the measured $\tilde{\tilde{n}}_z/\langle n_z \rangle$ profiles to the extended theory (8) which includes ICRH-driven minority effects. There is little change in the asymmetry for the HFS-heated case, with agreement slightly improved. A large impact for the LFS-heated plasma where by including the cyclotron heated minorities, $\tilde{\tilde{n}}_z/\langle n_z \rangle$ is predicted to be below zero. In Figure 8b, the extended theory is shown to accurately reproduce the inboard accumulation seen experimentally for the LFS-heated plasma.

The sensitivity of this result to the assumed minority fraction, f_m, is explored in Figure 9 where for $1\% < f_m$ 10% TRANSP simulations are repeated, and the $f_m(T_\perp/T_\parallel - 1)$ profile is plotted against minor radius. In the the circular limit (9), this factor is proportional to the n_{cos} term, and can be used as an estimate of the ICRH-driven asymmetry. The temperature anisotropy should be expect to be inversely related to the minority fraction, as lower f_m means higher rf power per particle, leading to a larger $T_\perp/T_\parallel$. This should result in a weak dependance of the in/out asymmetry on f_m, shown in the inset of Figure 9 in the region of r/a~0.5 where the largest ICRH-effect is observed experimentally. The value of $f_m(T_\perp/T_\parallel - 1)$ is shown to have a quadratic response to the minority fraction, making the agreement shown in Figure 8 relatively insensitive to the assumed n_m/n_e=4%. A more linear dependence with f_m is seen near r/a~0.25, and it is unclear what physics is driving the difference in response between this region and r/a ~ 0.5.

VI. DISCUSSION

Having a validated theory of parallel impurity transport is important in accurately interpreting information from modern tokamak diagnostics. The soft x-ray crystal spectroscopy technique used on C-

Mod to get core velocity and temperature profiles is also being planed for use on ITER [32] where neutral beam penetration at energies favorable for low-Z charge exchange diagnostics is weak. The ITER spectrometer plans to use intrinsic tungsten from divertor plasma facing components which could exhibit large asymmetries due to expected intrinsic rotation [33] and the mix of planned ion and electron cyclotron heating techniques. Spatial profile coverage is limited and an understanding of the poloidal variation of high-Z impurities will be crucial in obtaining accurate rotation and temperature profiles. Additionally, soft x-ray tomography is sometimes used [34,35] to aid in equilibrium reconstructions by assuming surfaces of constant emissivity are also flux surfaces. In plasmas where in/out asymmetries are expected, this can lead to systematic errors in the Shafranov shift.

Results presented in Section V demonstrate the sensitivity of the parallel transport of high-Z impurities to the poloidal electric field generated by ion cyclotron heating, suggesting measurements of $n_z(\theta)$ as general diagnostic technique to infer E_θ. The radial force balance equation is often used in a similar manner to determine the radial electric field [36]

$$E_r = \frac{-1}{Zen_z}\frac{\partial p_z}{\partial r} - v_{z,\theta}B_\phi + v_{z,\phi}B_\theta \quad (11)$$

where n_z, $\partial p_z/\partial r$ and $v_{z,\theta}$ and $v_{z,\phi}$ are all measured. In this case the poloidal electric field can be found from the parallel force balance equation, ignoring ion-impurity friction, via

$$E_\theta = \hat{b}\cdot\nabla\theta\frac{T_z}{e}\left[\frac{1}{Zn_z}\frac{\partial n_z}{\partial\theta} - \frac{m_z\omega^2}{2ZT_z}\frac{\partial R^2}{\partial\theta}\right] \quad (12)$$

Instead of radial pressure gradients and v_z being measured to find E_r, the parallel gradients and toroidal rotation, ω_z, can be used to find E_θ The presence of a poloidal electric field could impact cross-field transport by imparting a radial $E_\theta \times B_\phi$ drift. At r/a~0.5 the modeling shown in Figure 9b for the LFS-heated plasma that matches experiment, this results in drift velocity that varies over the flux surface ~ $v_d\sin\theta$ with $v_d \sim 3.5$ m/s as shown in Figure 10. No significant flux-surface averaged, radial particle flux will occur unless the density also had a non-zero up/down asymmetry. In this work, the main focus has been in/out asymmetry driven by minority heating and the centrifugal force, and future work will focus on ion-impurity friction effects which are responsible for the up/down asymmetry.

Neoclassical theories have shown that a poloidal potential variation of order the inverse aspect ration, $e\tilde{\phi}/T_e \sim \epsilon$, can impact transport by causing electrostatic trapping which complements the magnetic trapping inherent to the tokamak. It was shown that radial electron transport can, in some cases, be enhanced by a factor of 2 as $e\tilde{\phi}/T_e$ rises to $\sim 4\epsilon$ [11]. The bootstrap current can also be influenced by this modification to trapping with enhancement or reductions on the order of 20-30% depending on the sense

of the asymmetry and impurity content [12]. For the C-Mod case described above, the potential variation, $e[\phi(\theta)-\phi(0)]/T_e$ is plotted in Figure 10 where it is demonstrated to be much smaller than necessary to impact neoclassical transport. This demonstrates that high-Z impurity asymmetries can be used as a sensitive tool for measuring very small changes in the poloidal electric field. Large asymmetries, $\tilde{n}_z/\langle n_z \rangle \sim 1$, can act as a indicator of when neoclassical poloidal electric field effects need to be included in transport modeling.

Recent work studying the impact of poloidal asymmetries on anomalous radial impurity transport has shown that HFS accumulation of impurities can lead to a reduction or even a reversal of the impurity density zero flux gradient scale length [12,13]. The C-Mod measurements presented here show asymmetries, $\tilde{n}_z/\langle n_z \rangle \sim -0.15$, at the level where cross-field transport could be affected, and examples of $\tilde{n}_z/\langle n_z \rangle \sim -0.25$ have been observed in more recent in C-Mod plasmas. Future studies of asymmetry-induced turbulent impurity transport will require a more complete measurement of the poloidal variation of impurity density rather then just the in/out asymmetry. The existing tools [37,38] used to model the parallel transport for use with gyrokinetic codes include poloidal asymmetries driven by centrifugal force but do not include any poloidal electric field effects generated from cyclotron heating. Some extensions to these tools may be necessary to complete validation exercises for high-Z impurity transport in cyclotron-heated plasmas.

Although somewhat counter intuitive, it can be argued that it is easier to measure the poloidal variation of the high-Z impurity than the radial impurity density profile. This is due to the necessity of accurate electron density and temperature profiles as well as atomic physics modeling to turn an emissivity into an impurity density and constrain a 1-D impurity transport simulation. In contrast, the poloidal variation of the impurity emission can be determined from a SXR tomography diagnostic, a common tool on many tokamaks. It is suggested that future experimental investigations into high-Z impurity transport produce measures of the poloidal impurity density asymmetry. If large asymmetries are observed along with changes in radial transport, which can be caused by a variety of mechanisms, then parallel transport may be playing a role in radial transport.

VII. SUMMARY

Large, steady-state poloidal variations of high-Z impurity density are observed in Alcator C-Mod plasmas using hydrogen minority ICRH. Both inboard and outboard accumulation of molybdenum on a flux surface have been observed with $|\tilde{n}_z/\langle n_z \rangle|$ up to 0.3. Parallel impurity transport theories that include only inertial and ion-impurity friction forces, cannot explain rf heated C-Mod results. Significant

disagreement occurs on flux surfaces with cyclotron-heated energetic minority populations when the resonance layer is located at $R \geq R_o$. In these cases, inboard accumulation of molybdenum is observed. By measuring asymmetries during shot-to-shot scans of the minority resonance layer and examining the transient asymmetry response after removing the ICRH power, the link to cyclotron heating is firmly established. The effect is attributed to a poloidal potential variation sustained by magnetically trapped minority ions. Extensions to parallel impurity transport theory including this effect are derived, and are shown to agree qualitatively and quantitatively to measured asymmetries.

ACKNOWLEDGMENTS

The authors would like to thank S. M. Wolfe for the EFIT analysis tools, R. M. Churchill for assistance with diagnostic calibrations, D. Ernst for use of the fiTS software and the entire C-Mod team for excellent maintenance and operation of the tokamak. This work supported by US Department of Energy Agreement DE-FC02-99ER54512 and in part by an appointment to U.S. DOE Fusion Energy Postdoctoral Research Program administered by ORISE.

REFERENCES

[1] A. Loarte, *et al.* Nucl. Fusion. **47** S203 (2007)

[2] C. Angioni, *et al*. Phys. of Plasmas. **14** 055905 (2007)

[3] R. Guirlet, *et al.* Plasma Phys. Control. Fusion. **48** B63 (2006)

[4] M. Valisa, *et al*. Nucl. Fusion. **51** 033002 (2011)

[5] T. Hein and C. Angioni. Phys. of Plasmas. **17** 012307 (2010)

[6] T. Fülöp and H. Nordman. Phys. of Plasmas. **16** 032306 (2009)

[7] T. Fülöp and P. Helander. Phys. of Plasmas. **6** 3066 (1999)

[8] J.A. Wesson. Nucl. Fusion. **37** 577 (1997)

[9] M. Romanelli and M. Ottavian. Plasma Phys. Control. Fusion. **40** 1767 (1998)

[10] C.S. Chang. Phys. Fluids. **26** 2140 (1983)

[11] K. Indireshkumar and W.M. Stacey, Jr. Phys. Fluids B. **5** 1850 (1993)

[12] T. Fulop and S. Moradi. Phys. of Plasmas. **18** 030703 (2011)

[13] S. Moradi, *et al*. Plasma Phys. Control. Fusion. **53** 115008 (2011)

[14] H. Chen, *et al*. Phys. of Plasmas. **7** 4567 (2000)

[15] R. Dux, *et al*. Nucl. Fusion. **39** 1509 (1999)

[16] E. Marmer. Fusion Science and Technology. **51** 261 (2007)

[17] J.Y. Hsu, *et al*. Phys. Rev. Letters. **53** 564 (1984)

[18] W. Choe, *et al*. Phys. Plasmas. **2** 2044 (1995)

[19] L.C. Ingesson, *et al*. Plasma Phys. Control. Fusion. **42** 161 (2000)

[20] K. Marr, *et al*. Plasma Phys. Control. Fusion. 5**2** 055010 (2010)

[21] P.T. Bonoli, *et al*. Fusion Science and Technology. **51** 401 (2001)

[22] D.G. Whyte, *et al*. Nucl. Fusion. **50** 105005 (2010)

[23] N.P. Basse, *et al*. Fusion Science and Technology. **51** 476 (2001)

[24] A. Ince-Cushman, *et al*. Rev. Sci. Instrum. **79** 10E302 (2008)

[25] O. Sauter, *et al*. Phys. Plasmas. **6** 2834 (1999)

[26] M.L. Reinke and I.H Hutchsinson. Rev. Sci. Instrum. **79** 10F306 (2008)

[27] L.L. Lao *et al.* Nucl. Fusion **25** 1611 (1985)

[28] M.L. Reinke, *et al*. Rev. Sci. Instrum. **81** 10D736 (2010)

[29] K.B. Fournier, *et al.* Nucl. Fusion. **37** 825 (1997)

[30] K.B. Fournier, *et al.* Atom. Data and Nucl. Data Tables. **70**231 (1998)

[31] http://w3.pppl.gov/transp

[32] P. Beiersdorfer, *et al*. J. Phys. B: At. Mol. Opt. Phys. **43** 144008 (2010)

[33] J.E. Rice, *et al*. Nucl. Fusion. **47** 1618 (2007)

[34] E.T. Powell, *et al*. Nucl. Fusion. **33** 1493 (1993)

[35] J.P. Qian, *et al*. Nucl. Fusion. **49** 025003 (2009)

[36] K. Ida. Plasma Phys. Control. Fusion. **40** 1429 (1998)

[37] E.A. Belli and J. Candy. Plasma Phys. Control. Fusion. **51** 075018 (2009)

[38] R.A. Kolesnikov, *et al*. Phys. Plasmas. **17** 022506 (2010)

FIGURE CAPTIONS

FIGURE 1: EFIT equilibrium reconstruction of the typical plasma shape used in this experiment. The major radii of resonance layers for hydrogen minority ICRH are plotted for B_t=4.4, 4.7, 5.4 and 6.0 T. Tangency radii of the midplane AXUV diode arrays (open and closed circles - offset for clarity) are also plotted.

FIGURE 2: Radial profiles used in asymmetery modeling; (a) electron density, (b) electron temperature, (c) ion temperature and (d) toroidal rotation frequency.

FIGURE 3: Example AXUV emissivity profiles plotted against major radius (left) and normalized minor radius, r/a (right), demonstrating the presence of both inboard and outboard impurity accumulation for a LFS-heated plasma.

FIGURE 4: The poloidal varying impurity density profiles derived from the AXUV diode emissivity data for various ICRH resonance layer locations shown in Figures 1 and 2.

FIGURE 5: Comparison of measured (solid) and modeled (dashed black) impurity density asymmetries assuming only inertial effects for a B_t=4.4, HFS-heated plasma (a) and a B_t=6.0, LFS-heated plasma (b). Data are close to agreement for $r/a < 0.7$ in (a) but show significant disagreement between $0.3 < r/a < 0.65$ in (b) near the vicinity of the minority resonance layer.

FIGURE 6: At various r/a locations, the magnitude of the poloidal impurity density asymmetry versus toroidal field. B_t=5.4 puts the layer nominally on-axis with $B_t > 5.4$ T and $B_t < 5.4$ T being LFS- ($r/a > 0$) and HFS-heating ($r/a < 0$), respectively.

FIGURE 7: Time evolution of the measured impurity density asymmetry at r/a=0.5 and 0.7 (d) for the LFS-heated plasma. As the ICRH power (a) is ramped down faster than the energy confinement time, only small changes in the ion and electron temperature (b) are observed for the kinetic profiles. The measured asymmetries approach the modeling in Figure 5b, prior the to observed drop in core rotation (c), when measured asymmetries drop to zero.

FIGURE 8: Comparison of measurements (solid) with modeling (black dashed) impurity density

asymmetries combining the effect of the centrifugal force and cyclotron heating. For a HFS-heated plasma (a), including ICRH effects does not have a significant impact. For a LFS-heated plasma (b), the extended theory (8) is shown to agree well with measured in/out asymmetries.

FIGURE 9: Demonstration of the sensitivity of the ICRH-driven in/out asymmetry to the minority fraction, f_m. Near r/a~0.5 where the largest inboard impurity accumulation is observed, the asymmetry is shown to have a weak dependence on f_m, presumed to be driven by the drop in $T_\perp/T_\parallel$ as the minority fraction is increased.

FIGURE 10: Poloidal variation of the electrostatic potential, $e[\phi(\theta)-\phi(0)]/T_e$ (left axis) and the resulting ExB drift velocity (right axis) , calculated at r/a=0.45 from modeling shown in Figure 8b.

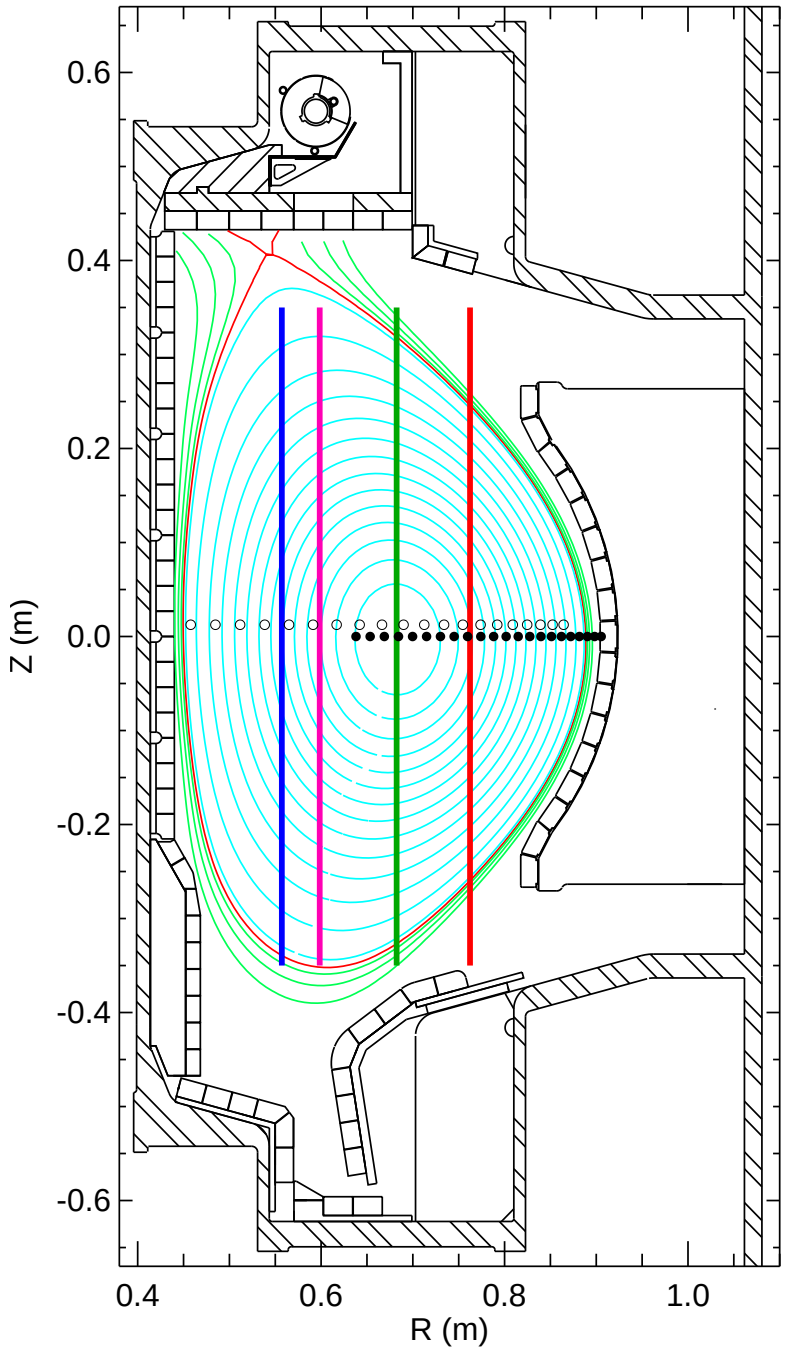

FIGURE 1

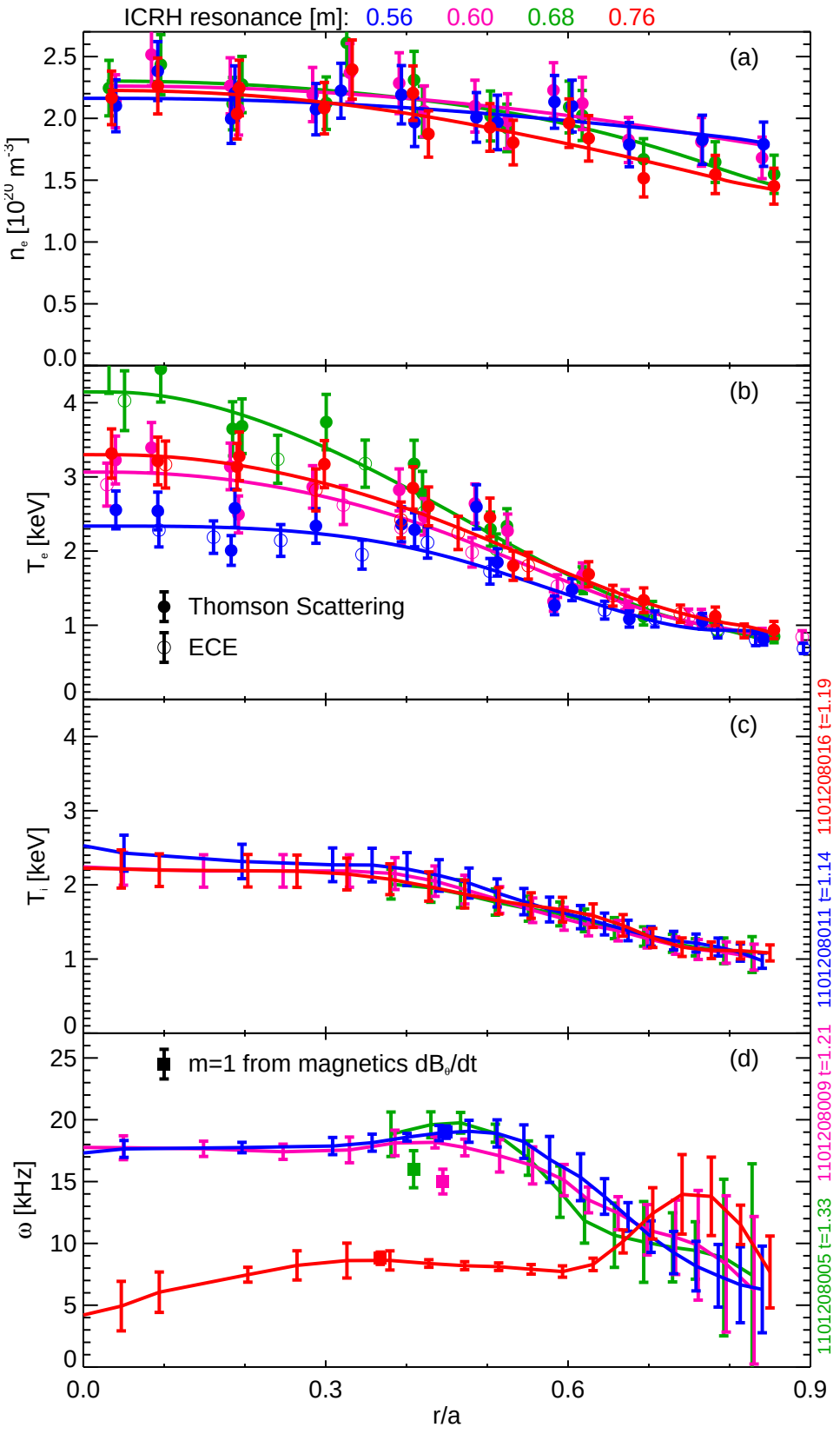
ICRH resonance [m]: 0.56 0.60 0.68 0.76
(a)
n_e [10^{20} m^{-3}]
(b)
T_e [keV]
Thomson Scattering
ECE
(c)
T_i [keV]
(d)
m=1 from magnetics dB_θ/dt
ω [kHz]
r/a
1101208005 t=1.33
1101208009 t=1.21
1101208011 t=1.14
1101208016 t=1.19

FIGURE 2

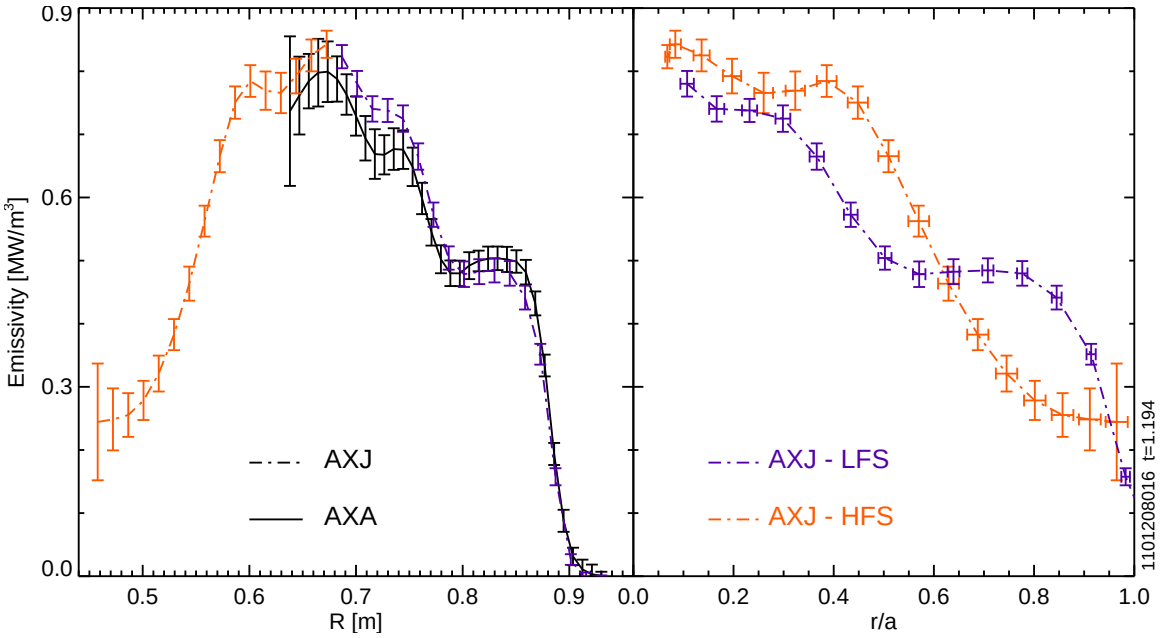

FIGURE 3

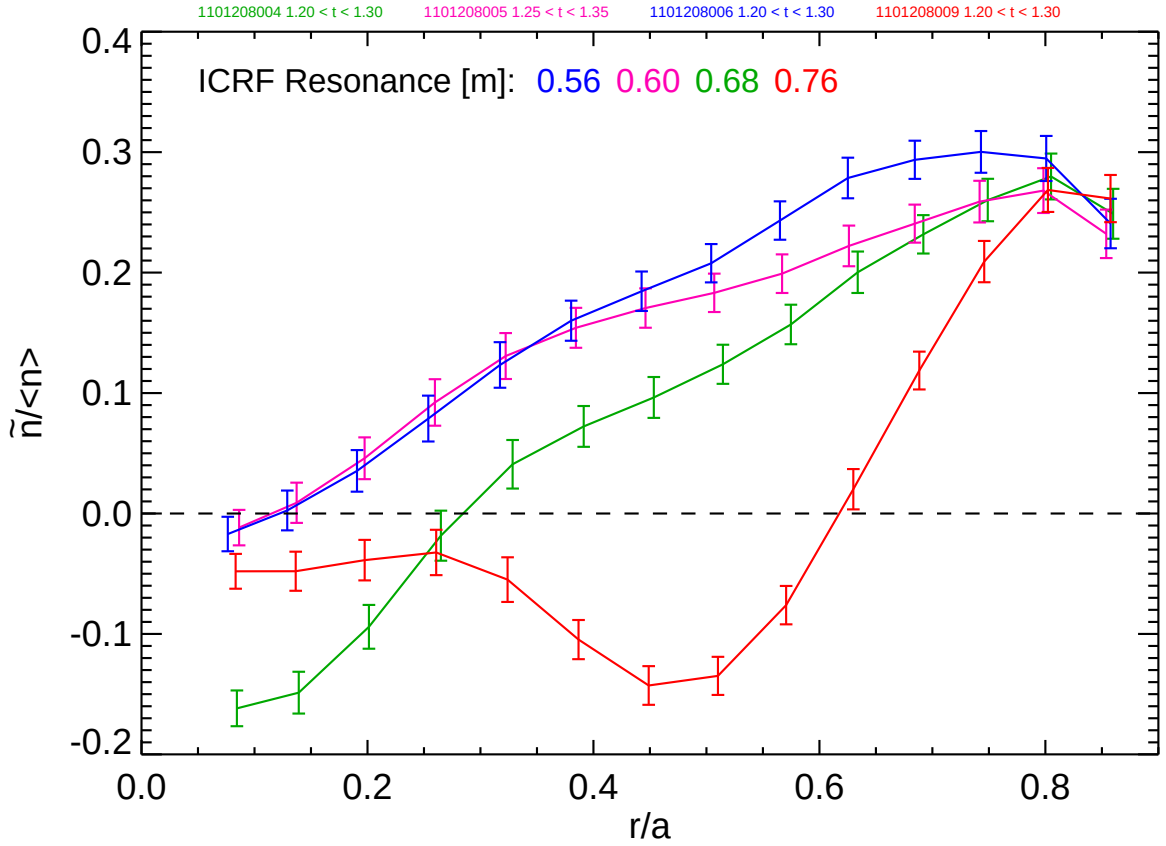

FIGURE 4

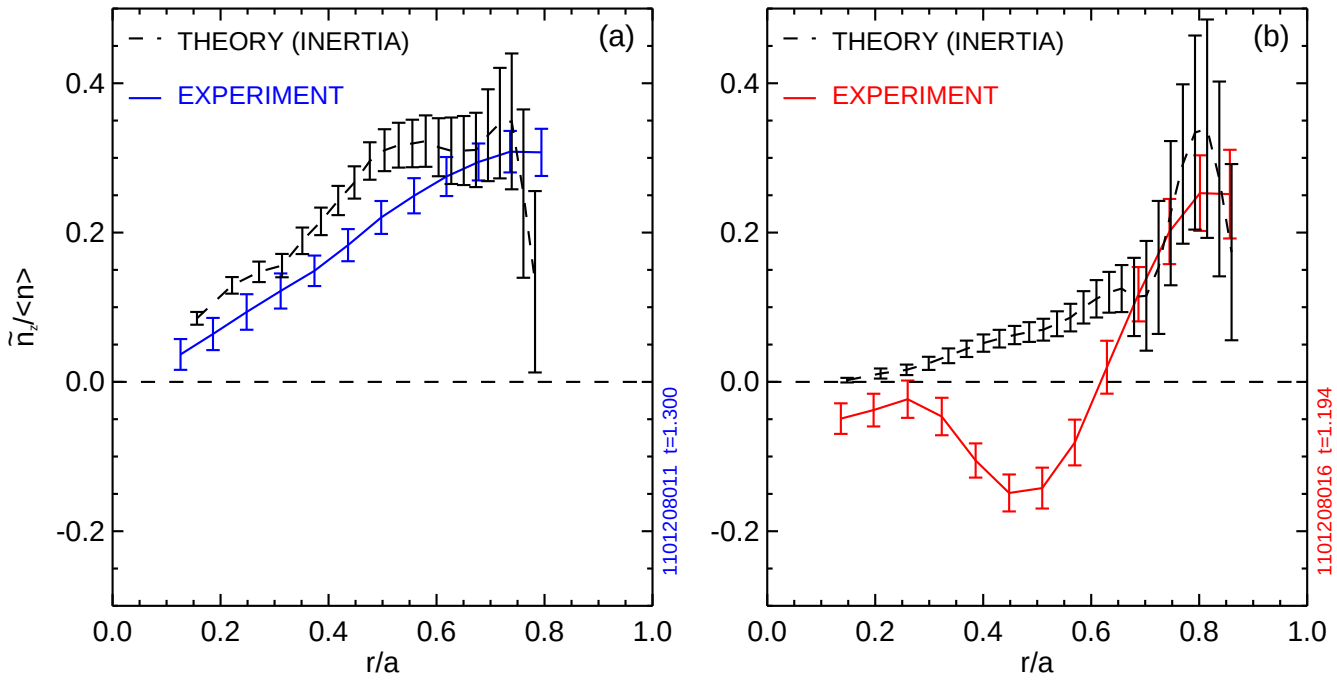
THEORY (INERTIA)
EXPERIMENT
(a)
(b)
$\tilde{n}_z/\langle n \rangle$
r/a
0.0
0.2
0.4
0.6
0.8
1.0
-0.2
1101208011 t=1.300
1101208016 t=1.194

FIGURE 5

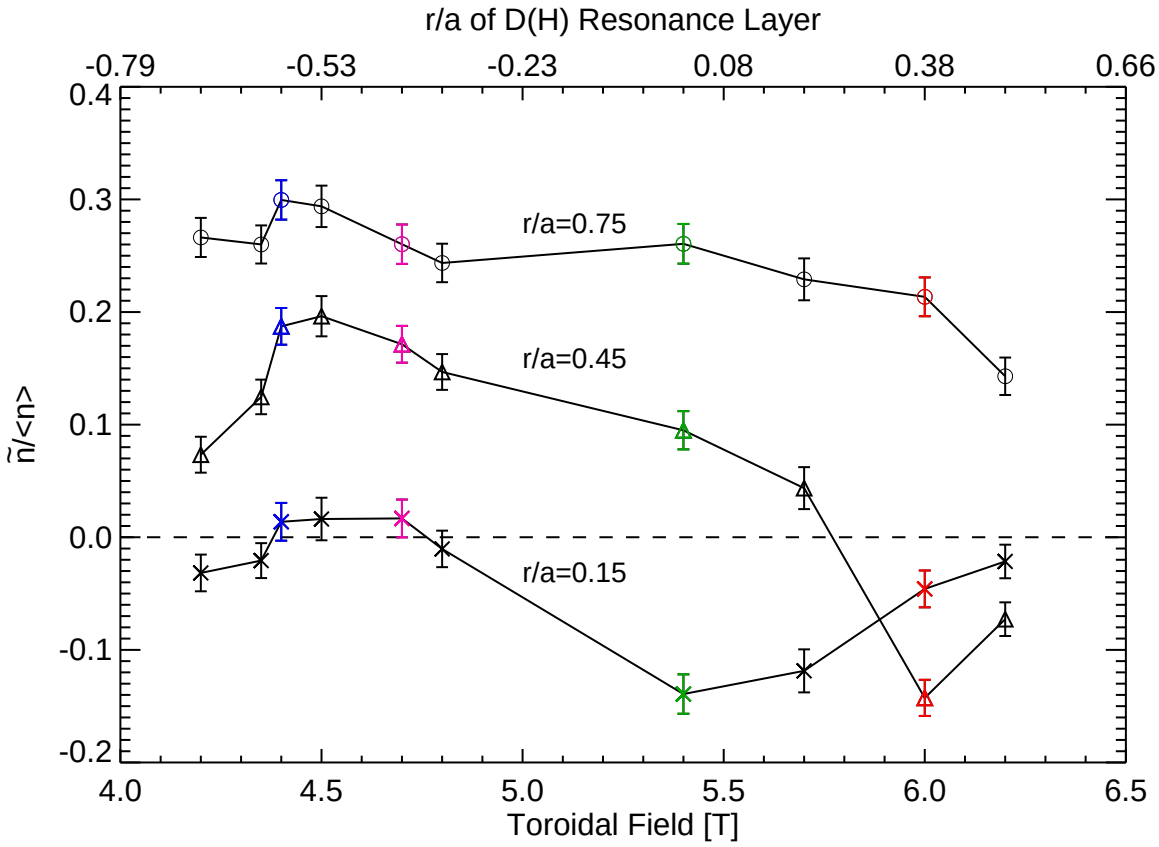
r/a of D(H) Resonance Layer
-0.79
-0.53
-0.23
0.08
0.38
0.66
0.4
0.3
0.2
0.1
0.0
-0.1
-0.2
r/a=0.75
r/a=0.45
r/a=0.15
ñ/<n>
4.0
4.5
5.0
5.5
6.0
6.5
Toroidal Field [T]

FIGURE 6

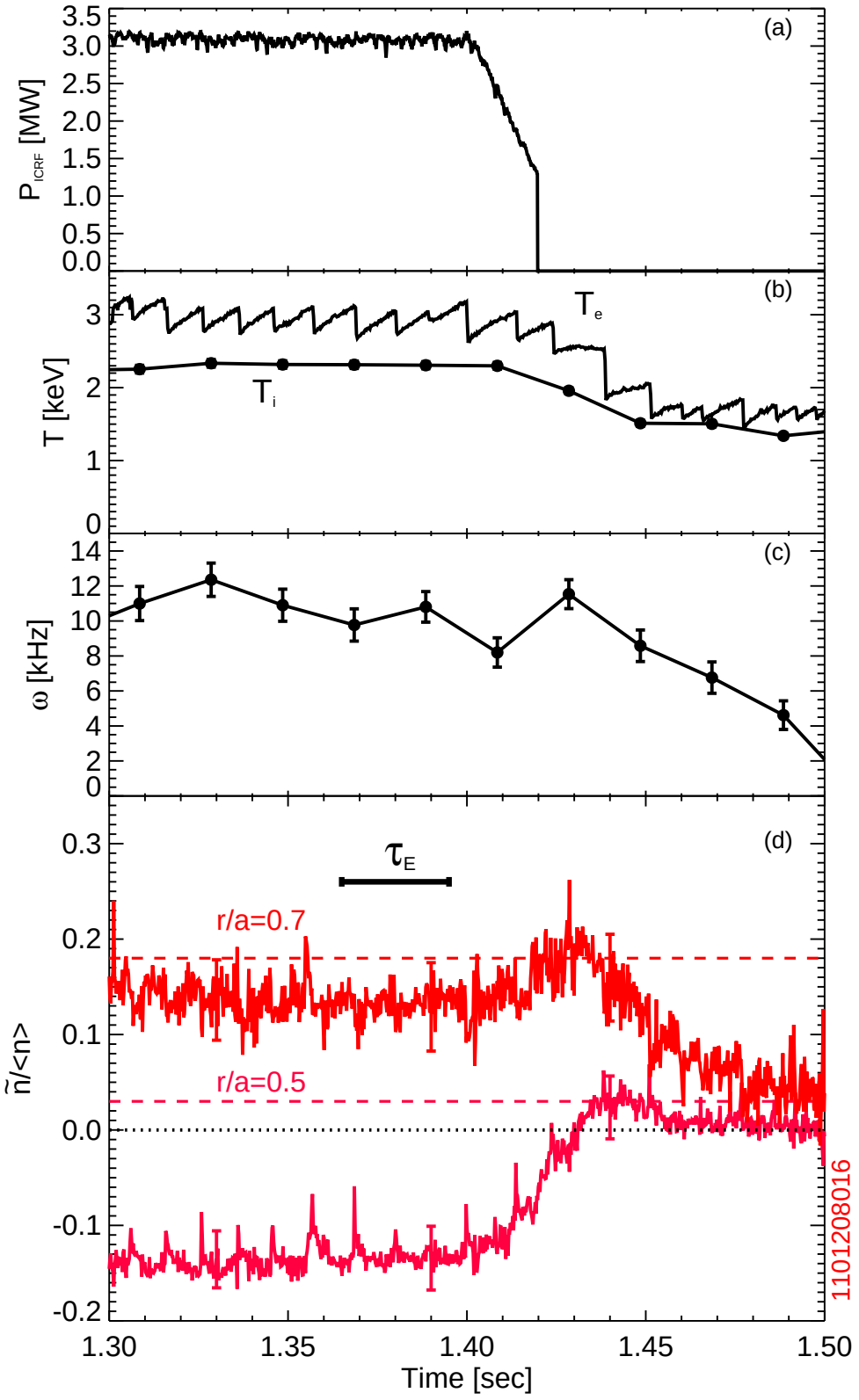
(a)
P_ICRF [MW]
3.5
3.0
2.5
2.0
1.5
1.0
0.5
0.0
(b)
T [keV]
T_e
T_i
3
2
1
0
(c)
ω [kHz]
14
12
10
8
6
4
2
0
(d)
τ_E
r/a=0.7
r/a=0.5
ñ/<n>
0.3
0.2
0.1
0.0
-0.1
-0.2
1101208016
1.30
1.35
1.40
1.45
1.50
Time [sec]

FIGURE 7

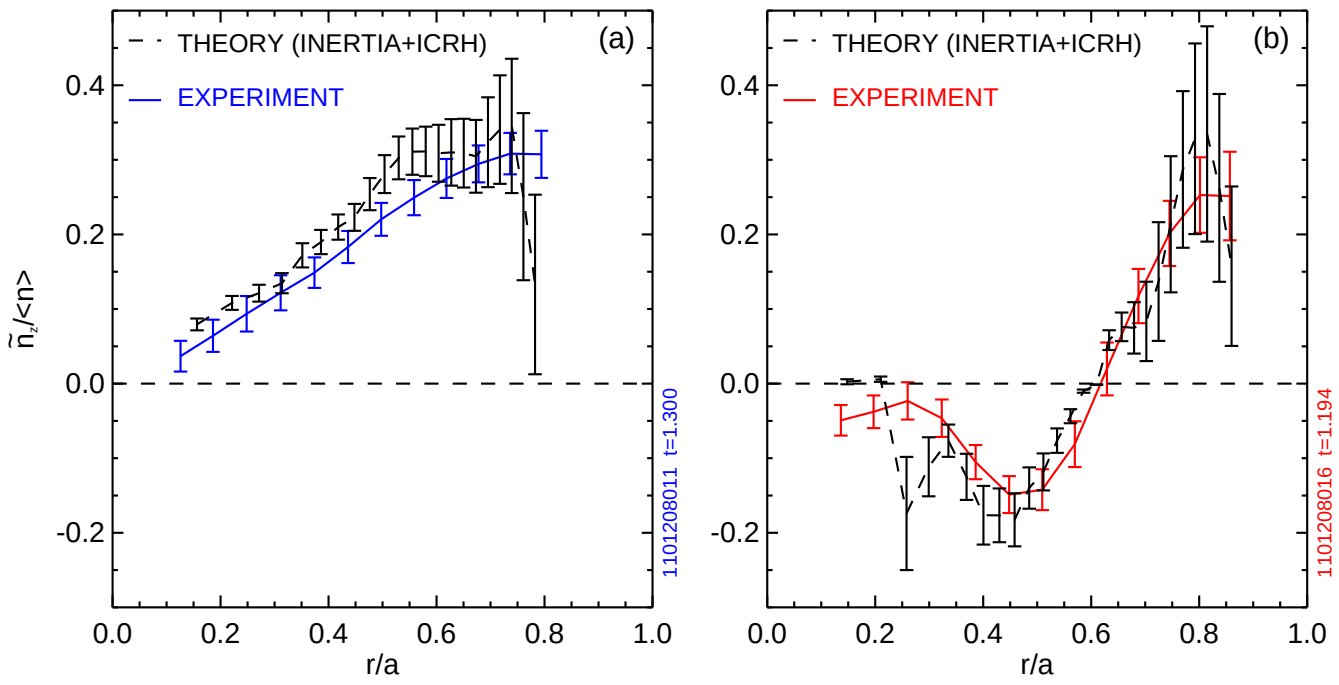
THEORY (INERTIA+ICRH)
EXPERIMENT
(a)
(b)
$\tilde{n}_z/<n>$
r/a
1101208011 t=1.300
1101208016 t=1.194

FIGURE 8

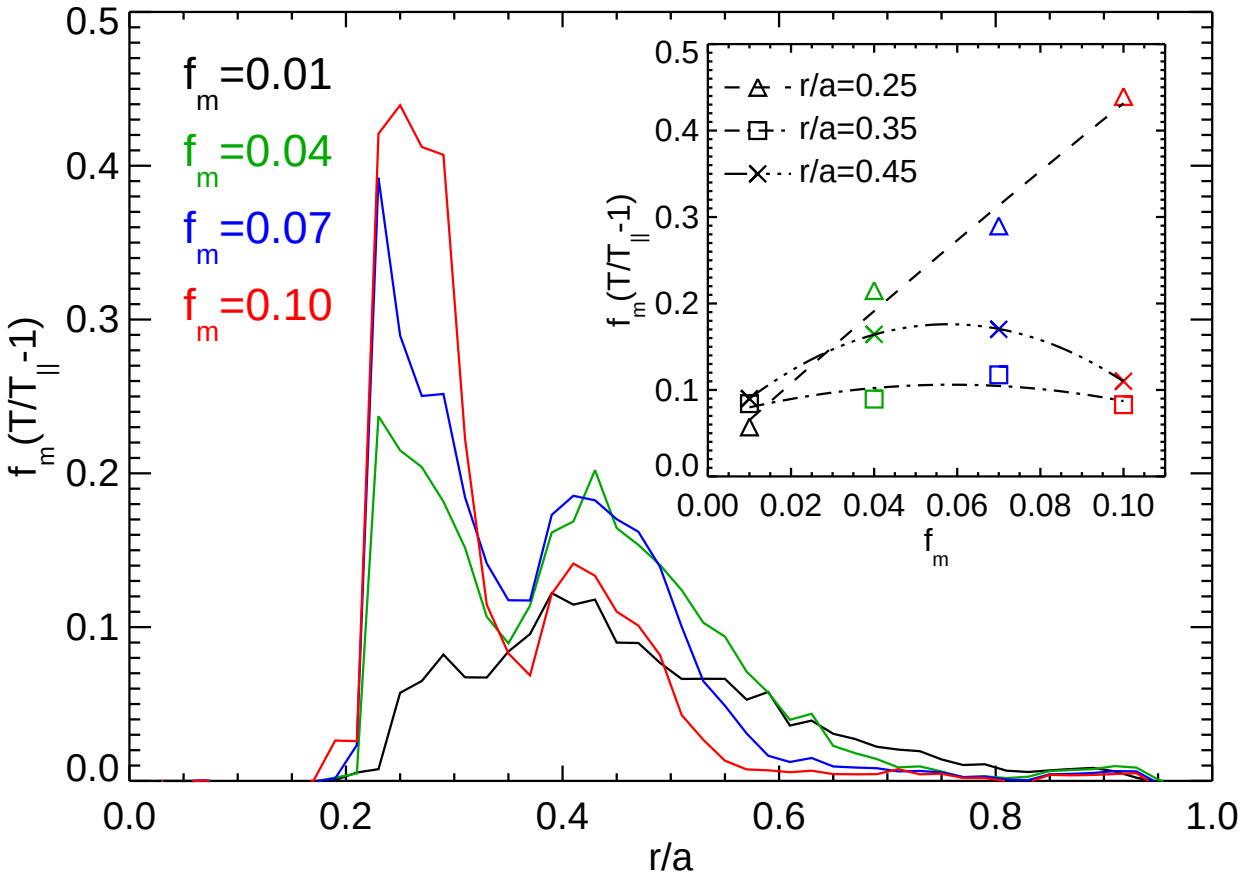
f_m=0.01
f_m=0.04
f_m=0.07
f_m=0.10
f_m(T/T_||-1)
r/a
0.0
0.1
0.2
0.3
0.4
0.5
0.6
0.8
1.0
r/a=0.25
r/a=0.35
r/a=0.45
f_m
0.00
0.02
0.04
0.06
0.08
0.10

FIGURE 9

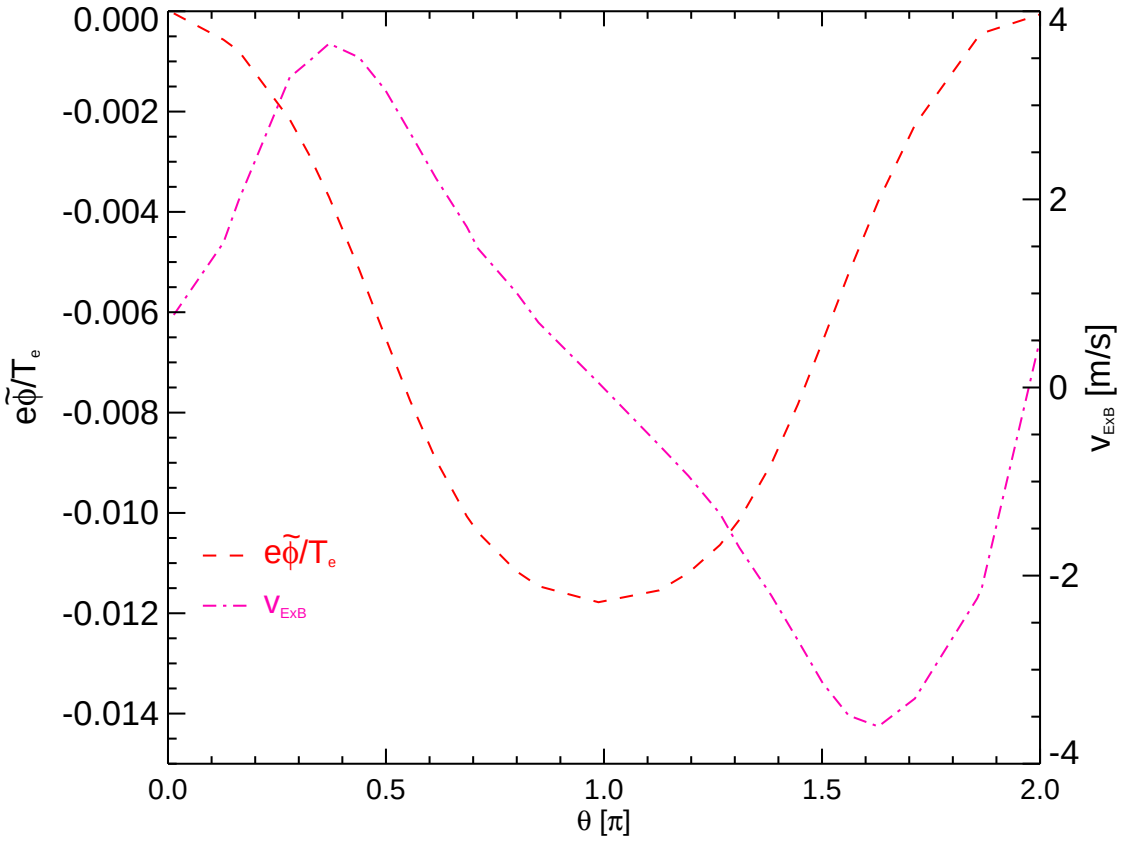
0.000
-0.002
-0.004
-0.006
-0.008
-0.010
-0.012
-0.014
4
2
0
-2
-4
0.0
0.5
1.0
1.5
2.0
θ [π]
eϕ̃/T_e
v_ExB [m/s]
eϕ̃/T_e
v_ExB

FIGURE 10